https://doi.org/10.5194/hess-2021-492
Preprint. Discussion started: 2 December 2021


Hydrology and Earth System Sciences
Discussions
Open Access

# Effects of passive storage on modelling hydrological function and isotope dynamics in a karst flow system in southwest China

Guangxuan Li[1,2], Xi Chen[1,2*], Zhicai Zhang[3], Lichun Wang[1,2], Chris Soulsby[4]

**Affiliations:**

[1] Institute of Surface-Earth System Science, School of Earth System Science, Tianjin University, Tianjin, China, 300072

[2] Tianjin Key Laboratory of Earth Critical Zone Science and Sustainable Development in Bohai Rim

[3] College of Hydrology and Water Resources, Hohai University, Nanjing, China

[4] School of Geosciences, University of Aberdeen, Aberdeen AB24 3UF, United Kingdom

[*] **Correspondence to:** xi_chen@tju.edu.cn

https://doi.org/10.5194/hess-2021-492
Preprint. Discussion started: 2 December 2021


Hydrology and Earth System Sciences
Discussions

**Abstract**

Representing passive storage in coupled flow-isotope models can facilitate simulation of mixing and retardation effects on tracer transport in many natural systems, such as catchments or rivers. However, the effectiveness of incorporating passive storages in models of complex karst flow systems remains poorly understood. In this study, we developed a coupled flow-isotope model that conceptually represents both "fast" and "slow" flow processes in heterogeneous aquifers to represent hydrological connections between hillslopes and low-lying depression units in cockpit karst landscapes. As this model originally included a varying number of passive storages at different positions of the flow system (e.g. fast/slow flow reservoirs combined with different hillslope/depression units), the model structure and relevant parameters were optimized using a multi-objective optimization algorithm. This was used to match detailed observational data of hydrological processes and isotope concentration in the Chenqi catchment in southwest China. Results show that the optimal structure for a coupled flow-isotope model incorporated only two passive storages in fast flow and slow flow paths of the hillslope unit. Using fewer or greater numbers of passive stores in the model could lead to under- or over-mixing of isotope signatures. This optimized model structure could effectively improve simulation accuracies for outlet discharge and isotope signatures, with >0.65 of the modified Kling-Gupta efficiency. Additionally, the optimal tracer-aided model yields reasonable parameter values and estimations of hydrological components (e.g. more than 80% of fast flow in the total discharge). Furthermore, results imply that the solute transport is primarily controlled by advection

https://doi.org/10.5194/hess-2021-492
Preprint. Discussion started: 2 December 2021



and hydrodynamic dispersion in steep hillslope unit, which is a remarkable phenomenon in the karst flow system. The study resulted in new insights, more realistic catchment conceptualizations and improved model formulation.

**Keywords:** Flow-isotope model; Passive storage; Karst flow systems; Chenqi catchment; Hillslope and depression units

https://doi.org/10.5194/hess-2021-492
Preprint. Discussion started: 2 December 2021



## 1 Introduction

The southwest China karst region is one of the world's largest continuous karst areas, covering ~540 $\times 10^3$ km$^2$ over eight provinces and providing water resources for more than 100 million people (Chen et al., 2018). Strong dissolution of carbonate rocks in the humid tropics and subtropics of southwest China creates unique cockpit karst landscapes, and complex surface and subsurface flow paths (e.g. sinkholes, caves and conduit networks) (Chen et al., 2018). The permeability is driven by fractures and varies over a large range depending on fracture aperture, density, orientation, and interconnectivity (Streltsova, 1976). This leads to great variability of hydrological and solute transport processes in space and time. Consequently, modeling hydrological and solute transport processes in this kind of karst systems is extremely challenging.

A wide range of hydrological models have been developed for karst areas, ranging from lumped models at the catchment scale to (semi-) distributed models with hydrological function parameterized for the grid-scales or landscape unit scales (Martínez‑Santos and Andreu, 2010; Hartmann et al., 2013). A key function of karst hydrological models is to capture the dual or multi-phase flows in a complex porous medium, capturing low velocities in the matrix and small fractures, as well as very high velocities in large fractures and conduits (White, 2007; Worthington, 2009). Model structures endowed with process-based conceptualization of the complex flow systems often lead to over-parameterization and large uncertainties for resulting simulation (Perrin et al., 2001; Beven, 2006). Incorporating additional field data from study catchments can provide information to better understand and improve model structures,

https://doi.org/10.5194/hess-2021-492
Preprint. Discussion started: 2 December 2021

Hydrology and Earth System Sciences
Discussions

constrain parameter ranges and efficiently reduce simulation uncertainties. In this regard, stable isotopes of water ($\delta^{18}O$ and $\delta^{2}H$) have been widely used to provide insight into the functioning of karst systems (Qin et al, 2017; Min et al, 2018; Elghawi et al, 2021), the mixing of water from different sources (Aquilina et al., 2006; Plummer et al., 1998), and the residence times of these sources (Batiot et al., 2003; Long and Putnam, 2004). In recent years, isotope-aided hydrological models have been developed to fully couple hydrological processes with stable isotope dynamics (Birkel and Soulsby, 2015). These coupled models are effective in understanding hydrological functions, such as water storage, flux, and age (Carey and Quinton, 2004; Chacha et al., 2018), which are useful metrics to characterize the karst critical zone.

In the vast majority of hydrological models, flow routing is driven by pressure gradients, creating a dynamic (active) water storage which are influenced by water balance considerations (Fenicia et al., 2010; Soulsby et al., 2011), while isotopes (or any conservative solute) are subject to advection at much slower velocities along the actual flow paths of water where mixes occur through dispersion and diffusion (Hrachowitz et al., 2013). The tracer mixing and transport can potentially create an additional volume (the passive storage) for storage components below field capacity (Birkel et al., 2011) in the unsaturated zone and at depths far below stream or water table in the saturated zone. Hence, the storage volume for the isotope mixing and transport consists of the active storage and the passive storage. The conceptual

https://doi.org/10.5194/hess-2021-492
Preprint. Discussion started: 2 December 2021




combination of active storage with passive storage in isotope-aided hydrological models enhances solute mixing and resultant tracer retardation.

In the southwest karst region of China, a few studies have recently incorporated passive storage into coupled flow-isotope models for simulating hydrological and solute transport processes. For example, Zhang et al. (2019) developed a semi-distributed conceptual model for capturing discharge and isotope dynamics in the Chenqi catchment. The model has a function for passive storage to affect isotope mixing only within the conceptual hillslope unit, but it did not incorporate any passive storages in the fast and slow reservoirs for the depression unit. Chang et al. (2020) compared the lumped model structures with different connections of epikarst and the underlying slow and fast reservoirs according to observations of the spring discharge and electrical conductivity (EC) at Yaji catchment of southwest China. They set a passive storage for the fast flow reservoir and neglected passive storage in the slow flow system based on assumption that EC in the slow system can always reach its maximum value or equilibrium state at each time step.

Nevertheless, these studies have not systematically analyzed how the configuration of passive storage functions in the model structure constrains simulations of hydrological processes and isotope dynamics for karst flow systems. Particularly, the effects of passive storage structures are underexplored in terms of the location and number of passive storages needed for fast and/or slow flow reservoirs in hillslope and/or depression units, respectively. Consequently, it remains unclear what is the most

https://doi.org/10.5194/hess-2021-492
Preprint. Discussion started: 2 December 2021

Hydrology and Earth System Sciences
Discussions
Open Access

efficient way of incorporating passive storage into coupled flow-tracer simulations. Moreover, there is no clear consensus on how to conceptualise mixing mechanisms within and between active and passive storages. For example, Ala-Aho et al. (2017) used complete mixing to represent the water and tracer exchange flux between passive storage and active storage in model cells for three experimental catchments, though this gave partial mixing at the catchment-scale. In contrast, Page et al. (2007) used a static partial mixing mechanism in the hydrochemistry module of a conceptual model for simulating stream chloride concentrations in two subcatchments at Plynlimon, Wales. Hrachowitz et al. (2013) introduced a dynamic partial mixing mechanism to better quantify water, tracer fluxes and associated water age distributions of a catchment in Scotland. In southwest China karst catchments, Zhang et al. (2019) assumed static partial mixing between passive storage and active storage in hillslope response units. Meanwhile, Chang et al. (2020) used complete mixing between passive storage and active storage in the fast flow reservoir. In short, adding passive storage for the isotope (solute) mixing calculation often seems arbitrary in previous studies. Meanwhile, additional functions of passive storage in the models can further complicate the model structure and add parameters (Capell et al., 2012; Hrachowitz et al., 2013; Rodriguez et al., 2017), which might eventually increase uncertainty over modelled water flux and isotope dynamics.

The aim of this study is to evaluate the effectiveness of alternative ways of incorporating passive storage into fast/slow flow reservoirs in hillslope/depression units

https://doi.org/10.5194/hess-2021-492
Preprint. Discussion started: 2 December 2021

Hydrology and Earth System Sciences
Discussions

for improving stream discharge and stable isotope simulations. The study focuses on the Chenqi catchment, in the karst of southwest China using high resolution observations of hydrological and stable isotope data. We developed a coupled flow-isotope model that can quantify and capture fast and slow flow responses to rainfall as well as hydrological connections between hillslope and depression units. The functions of passive storage on stream flow and stable isotope simulations were comprehensively evaluated; by comparing numerical results from models with a varying number of passive stores located in hillslope and/or depression units. Ultimately, an appropriate model structure is suggested that can most efficiently describe hydrological functioning in the study catchment.

## 2 Study area and data descriptions

### 2.1 Study area

The small karst catchment of Chenqi is located in the Puding Karst Ecohydrological Observation Station, Guizhou Province of southwest China (Fig. 1). Chenqi is characterized by a subtropical monsoon humid climate with a mean annual temperature of 14.2℃, mean annual rainfall of 1140 mm, and mean annual humidity of 78%. Precipitation mainly occurs in the rainfall season (May-August), accounting for more than 80% of the annual amount. The catchment is a typical karst peak cluster landform where a central depression is surrounded by hillslopes. Considering the distinct features of hillslope and depressions, the catchment is divided into two geomorphic units: hillslope and depression, with an area of 0.73 and 0.17 km$^2$, respectively (Table 1).

https://doi.org/10.5194/hess-2021-492
Preprint. Discussion started: 2 December 2021



Specifically, the hillslopes of the Chenqi catchment are steep with elevations ranging from 1340m to 1530m. The soil layer in the hillslope unit is thin (<50 cm) and irregularly distributed. Outcrops of carbonate rocks cover 10~30% of the catchment. The soluble bedrock is mainly composed of marl, thick limestone, thin limestone, and dolomite. Field investigations have shown a rich fracture zone (epikarst) on hillslopes (Fig. 1d) which has a thickness of 7.5~12.6 m, generally becoming shallower in an upslope direction (Zhang et al., 2011). Deciduous broadleaved forests and shrubs are mostly grown on the upper and middle parts of hillslopes, and corn is grown at the low of the gentle hillslopes (Chen et al., 2018). In contrast, in the flat depression, the accumulated soils are thick (~200 cm) and cultivated for crops of corn and rice paddy.

The drainage system includes an intermittent surface water channel and a perennially flowing underground conduit connecting the hillslopes to the catchment outlet. The flow discharge response to rainfall is fast, characterized by a sharp rise and decline of hydrographs. Zhang et al. (2013) found that the response time lag of fast (quick) flow to precipitation is very short (4~9 h) by studying the hydrological process of two epikarst springs in the upper catchment.

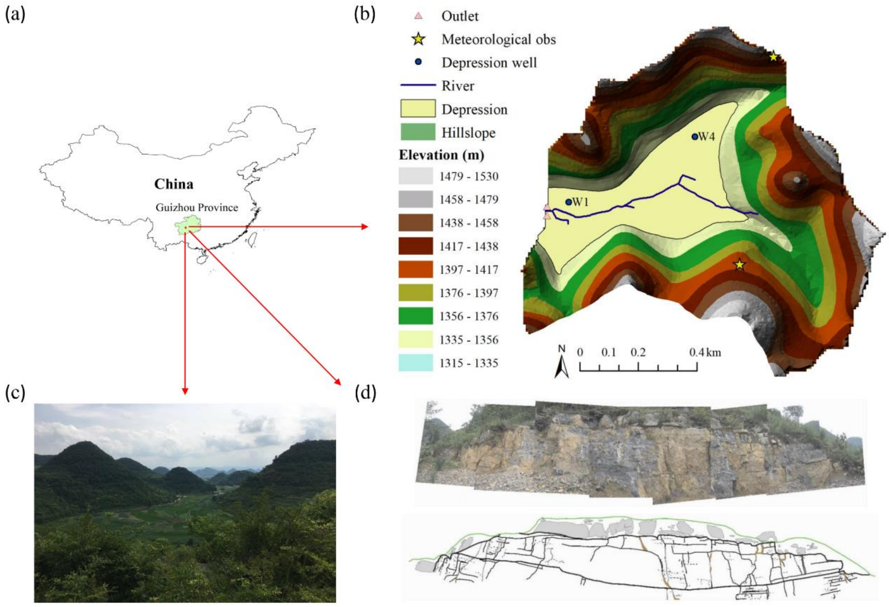


**Figure 1.** The location of Chenqi catchment (a), topography (b), photo (c) and a typical fracture profile (d).

**Table 1**. The catchment characteristics of two landscape units at Chenqi

| | Hillslope | Depression |
|---|---|---|
| Area (km²) | 0.73 | 0.17 |
| Elevation (m.a.s.l.) | 1340~1530 | 1315~1340 |
| Soil thickness | <0.5 m | >2 m |
| Land cover and use | Forest (13.67%), shrub (30.38%), grass (12.26%) and crops (40.1%) | |

## 2.2 Observational dataset

In the Chenqi catchment, an automatic meteorological station (Fig. 1b) was installed to record rainfall, temperature, air pressure, wind speed, humidity, and solar radiation. These data were used to calculate the potential evaporation via the Penman formula. Discharge at hillslope springs and the catchment outlet were measured by v-notch weirs

https://doi.org/10.5194/hess-2021-492
Preprint. Discussion started: 2 December 2021



with a time interval of 15 min. All observational datasets were collected from October 8th 2016 to June 12th 2018.

In particular, hillslope springs, flows at the catchment outlet, and rainfall were regularly sampled at daily intervals. They were intensively sampled during the wet season (May-August) using an autosampler set at an hourly interval. In total, we collected 253 rainfall samples, 1095 hillslope spring samples and 1096 water samples at the catchment outlet of underground channel (Table 2). Groundwater was also sampled from two depression wells (Fig. 1b) at depths varying between 13 ~ 35 m below the ground surface during four rainfall events. The water samples were tested and analyzed by the MAT 253 laser isotope analyser (instrument precision was ± 0.5 ‰ for δD and ± 0.1 ‰ for $\delta^{18}O$) at the State Key Laboratory of Hydrology and Water Resources of Hohai University.

Our measurements clearly show that the mean values of δD and $\delta^{18}O$ (Table 2 and Fig. 2) change to be enrichment in the following order: the hillslope spring, the depression groundwater and the catchment outlet discharge. This implies mixing with “old” water over the course of water flow paths from the hillslopes towards the outlet (Zhang et al., 2019; Zhang et al., 2020). In the depression, the mixing with “old” water is enhanced from the hillslope foot to the outlet as the isotope values of groundwater W4 close to the hillslope spring are more negative than those of groundwater W1 near the catchment outlet (Fig. 2 and Table 2).

https://doi.org/10.5194/hess-2021-492
Preprint. Discussion started: 2 December 2021



As shown in Fig. 2, when plotted in dual isotope space, the data points of the δD ~ $\delta^{18}$O regression line for the hillslope spring and the outlet discharge approach to the two regression lines controlled by the new water of rainwater and old groundwater of depression W1, respectively. This underlines previous insights that the catchment flow system is be composed of flows with varying response times (or groundwater age), namely the new fast flow and old slow flow (Zhang et al., 2019). The contribution of the fast and slow flow components to the catchment outlet enlarges the isotope variability of the outlet discharge (e.g., larger coefficient of variation (CVs) in Table 2). This enlarged isotope variability of the outlet discharge is mostly attributed to that of the hillslope spring since their temporal variations of δD and $\delta^{18}$O are consistent (Fig 3), and their ranges of δD and $\delta^{18}$O are close (Table 2 and Fig 2).

The mean lc-excess value (lc-excess=$\delta D - a \cdot \delta^{18}O - \beta$ in Table 2) in the study period shows that the evaporative effect on the hillslope spring is strong. The strong evaporative effect results in continuous enrichment in heavy isotopes of the hillslope spring in the dry season from November to April (Fig 3). In the wet season from May to October, howeve, the lc-excess values do not represent any trends while the δD of the hillslope spring is gradually depleted. This phenomenon indicates that with the increase of precipitation input, the hillslope spring receives fresh water from the rainfall recharge. The variations of the δD and lc-excess values of the catchment outlet discharge generally agree with those of the hillslope spring, which again indicate that the outlet discharge is mainly dependent on the hillslope spring.

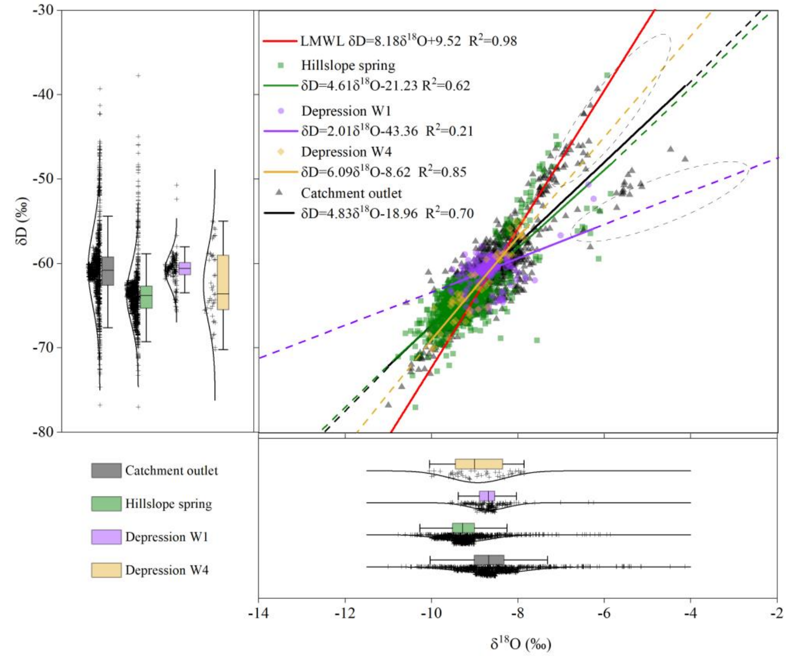


**Figure 2.** Plots of $\delta^{18}$O-δD for rainwater, catchment outlet discharge, hillslope spring and depression groundwater at wells W1 and W4

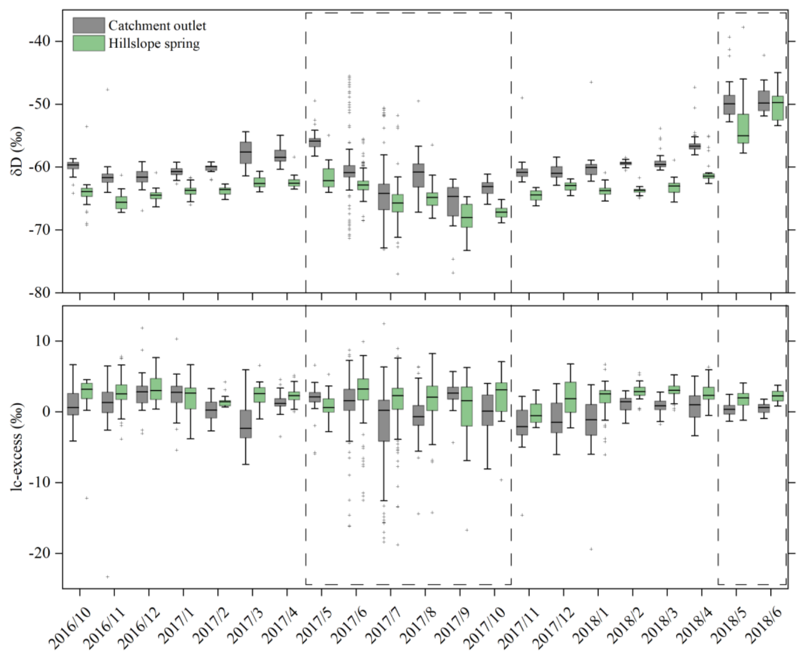


225 **Figure 3.** Monthly observed δD and lc-excess of outlet discharge and hillslope spring during the study period.

https://doi.org/10.5194/hess-2021-492
Preprint. Discussion started: 2 December 2021



**Table 2**. Characteristics of isotope data for rainfall, hillslope spring, catchment outlet discharge and depression groundwater

| Obs | Numbers | $\delta$D (‰) | | | $\delta^{18}$O (‰) | | | lc-excess | |
|---|---|---|---|---|---|---|---|---|---|
| | | Range | Mean | CV | Range | Mean | CV | Range | Mean |
| Rainfall | 253 | -120.2~29 | -64.9 | 0.49 | -16.6~1.0 | -9.1 | 0.42 | -16.71~17.37 | -0.04 |
| Catchment outlet discharge | 1096 | -76.8~-39.3 | -60.6 | 0.07 | -11~-4.1 | -8.6 | 0.09 | -23.31~12.45 | 0.33 |
| Hillslope spring | 1095 | -77~-37.8 | -63.7 | 0.05 | -10.8~-5.9 | -9.2 | 0.06 | -18.77~9.92 | 2.06 |
| Groundwater W1 | 175 | -65.7~-50.7 | -60.8 | 0.03 | -9.6~-6.3 | -8.7 | 0.05 | -10.75~7.6 | 0.65 |
| Groundwater W4 | 47 | -70.2~-55 | -62.5 | 0.07 | -10.1~-7.9 | -8.9 | 0.07 | -3.56~6.51 | 0.96 |

## 3 Model development

### 3.1 Conceptual model structure

Considering the contrasting features of catchment landscapes, the model structure can be conceptualized by focusing on the hydrologic connectivity of the "hillslope-depression-stream" continuum (Fig. 4) (Zhang et al., 2020). That is, the catchment area is divided into hillslope and depression units, each unit can be vertically separated into an unsaturated zone in the upper soil and epikarst layers and a saturated zone representing the deep aquifer (Fig. 4). To quantify diffusive and concentrated allogenic and autogenic recharge in each unit, the unsaturated zone is partitioned into two media: the low permeability zone of soil matrix and small fractures ($\alpha$), and high permeability zone of large fractures and swallow holes (1-$\alpha$). Rainfall falling on the low permeability area ($\alpha$) replenishes any moisture deficits first and then generates runoff (free water) when moisture reaches field capacity. This then recharges into deep groundwater

https://doi.org/10.5194/hess-2021-492
Preprint. Discussion started: 2 December 2021

Hydrology and Earth System Sciences
Open Access
Discussions

through diffusive and concentrated allogenic and autogenic recharge. Rain falling on the high permeability area (1-α) directly enters underground channels through upper sinkholes commonly found in carbonate aquifers (Worthington, 2009). The groundwater aquifer is separated into a fast flow reservoir and slow flow reservoir that is interconnected by flow exchange driven by the prevailing hydraulic gradient between two reservoirs (Hartmann et al., 2013; Zhang et al., 2019).

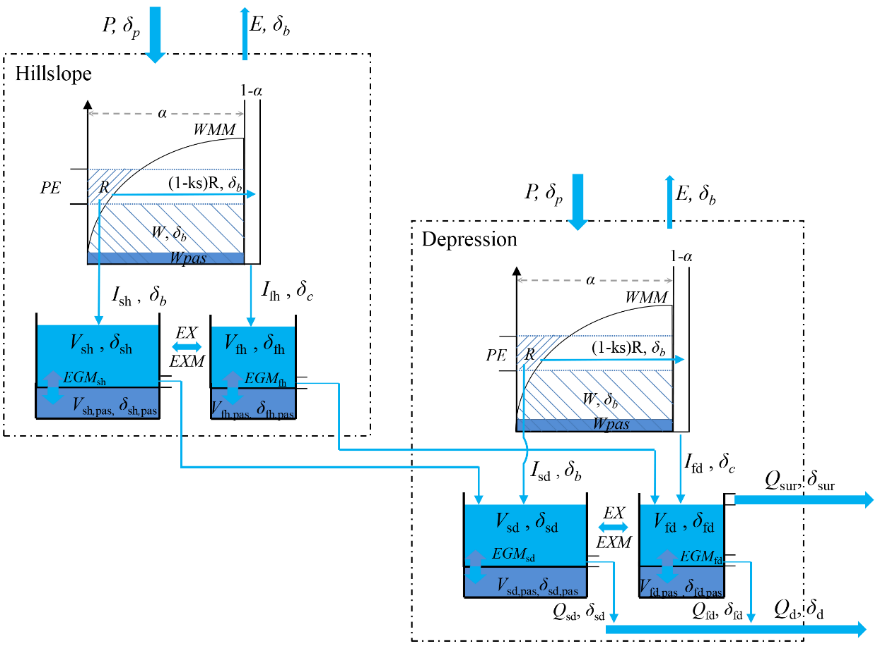


**Figure 4.** Conceptualized structure for the coupled flow-isotope model. The light blue shades indicate active storage, the dark blue shades indicate passive storage. The detailed descriptions of the model parameters are shown in Table 4.

### 3.1.1 Hydrological routing

In the matrix or small fracture area (α), which is considered as the recharge pathway to the slow flow reservoir, the spatial heterogeneity of storage volumes can be described by a set of compartments like the VarKarst model (Hartmann et al., 2013) and a

https://doi.org/10.5194/hess-2021-492
Preprint. Discussion started: 2 December 2021


Hydrology and Earth System Sciences
Open Access
EGU
Discussions

distribution curve of the storage capacity like the Xinanjiang model in Fig. 4 (Zhao, 1992) following:

$$\frac{f}{F} = 1-(1-\frac{wm'}{WMM})^{b} \tag{1}$$

where $f$ represents free water yield area, $F$ represents the total of the area (α), $wm'$ is the areal mean tension water storage at $f$, $WMM$ is the maximum value of $wm'$, and $b$ is a parameter.

Based on Eq. (1), the initial areal average storage $W$ is an integration of $wm'$ within 0~$A$ in the area (1-f/F) :

$$W = \int_0^A (1-\frac{wm'}{WMM})^{b} dwm' = \frac{WMM}{1+b}\left[(1-\frac{A}{WMM})^{1+b}\right] \tag{2}$$

when $A$=$WMM$, the storage in the entire area reaches the storage capacity. Thus, the mean storage capacity $wm$ is equal to $\frac{WMM}{1+b}$ (Zhao, 1992).

When the net precipitation $PE$ ($PE$=$P$-$E$)>0 and if $P$-$E$+$A$<$WMM$, the water yield $R$ is：

$$R = P-E-wm+W+wm(1-\frac{P-E+A}{WMM})^{1+b} \tag{3}$$

Note that $P$ is precipitation and $E$ is actual evaporation estimated by $E = kc \cdot Ep \cdot \frac{W}{wm}$, in which $kc$ is a coefficient for evapotranspiration, and $Ep$ is potential evapotranspiration.

If $P$-$E$+$A$≥$WMM$, the water yield $R$ is：

$$R = P-E-wm+W \tag{4}$$

Most of the water yield $R$ in the matrix or small fracture area (α) recharges into the underlying slow flow reservoir (i.e., $I_s = ks \cdot R \cdot \alpha$, where $ks$ is a scaling coefficient less than 1). The remaining runoff ((1-*ks*)$I_s$) together with rainfall $P$ falling on the swallow holes (1-α) directly recharges into fast flow reservoir (i.e., $I_f$=$P$(1-α)+$R$(1-*ks*)α).

Consequently, the water balance in the fast and slow reservoirs is:

$$\frac{dV_s}{dt} = I_s - EX - Q_s \tag{5}$$

$$\frac{dV_f}{dt} = I_f + EX - Q_f \tag{6}$$

where $V_s$ and $V_f$ are storages of slow and fast flow reservoirs, respectively; $Q_s$ and $Q_f$ are discharges from slow and fast reservoirs, respectively; $EX$ is flux between fast flow and slow flow reservoirs.

$EX$ is estimated by difference of the saturated storages (or water heads) between the fast flow and slow flow reservoirs (i.e., $EX=ke(V_s-V_f)$), where $ke$ is a coefficient of exchange flux between the slow and fast flow reservoirs). $Q_s$ and $Q_f$ are estimated according to the linear relationship between storage $V$ and discharge (i.e., $Q_s=\eta s \cdot V_s$, and $Q_f = \eta f \cdot V_f$, where $\eta s$ and $\eta f$ are outflow coefficients of slow and fast flow reservoirs, respectively).

### 3.1.2 Isotopic concentration routing

The mass balance in the unsaturated zone storage can be expressed as:

$$\frac{d(WU\delta_b)}{dt} = P\delta_p - R\delta_b - E\delta_b \tag{7}$$

where $WU$ ($WU=W+W_{pas}$) is the moisture storage consisting of active storage $W$ or mobile water (Sprenger et al., 2017; Sprenger et al., 2018) and passive storage $W_{pas}$, $\delta_p$ and $\delta_b$ are the stable isotope concentrations of rainwater ($P$) and moisture (and water yield $R$), respectively. Eq. (7) assumes instantaneous mixing of rainwater ($P$), water

https://doi.org/10.5194/hess-2021-492
Preprint. Discussion started: 2 December 2021


Hydrology and Earth System Sciences
Discussions
Open Access

yield ($R$) and soil moisture ($W$), and complete mixing of the active storage ($W$) with passive storage ($W_{pas}$) in the area ($\alpha$) since soils are very thin.

As a portion of the water yield ($I_s$) recharges into the deeper aquifer, the mass balance for the slow flow reservoir is

$$\frac{d(V_s\delta_s)}{dt} = I_s\delta_b - EXM - EGM_s - Q_s\delta_s \tag{8}$$

where $EXM$ is the exchange mass between the slow flow and fast flow reservoirs (estimated by $ke(V_s\text{-}V_f)\delta_s$ for $EXM$>0, and $ke(V_s\text{-}V_f)\delta_f$ for $EXM$<=0), and $EGM_s$ represents the mixing of the solute between the active ($V_s$) and passive ($V_{s,\,pas}$) storages for the slow flow reservoir ($=\varphi_s V_s(\delta_s - \delta_{s,\,pas})$, where $\varphi_s$ is the exchange coefficient between the active and passive storages for slow flow; $V_{s,\,pas}$ and $V_{f,\,pas}$ are the passive storage of slow flow and fast flow reservoirs, respectively; $\delta_{s,\,pas}$ and $\delta_{f,\,pas}$ are the stable isotope $\delta$ of passive storage for the slow flow and fast flow reservoirs, respectively.

Similarly, the mass balance for the fast reservoir is

$$\frac{\mathrm{d}(V_f\delta_f)}{dt} = I_f\delta_c + EXM - EGM_f - Q_f\delta_f \tag{9}$$

where $EGM_f$ ($=\varphi_f V_f(\delta_f - \delta_{f,\,pas})$) is the mixing of solute between active ($V_f$) and passive ($V_{f,\,pas}$) storages for the fast flow reservoir, $\varphi_f$ is exchange coefficient between active and passive storages for fast flow, and $I_f\delta_c$ is the recharge water mass, equal to

$$I_f\delta_c = P\delta_p(1-\alpha) + \delta_b R(1-ks)\alpha \tag{10}$$

The mass balance of the passive storage ($V_{pas}\,\delta$) for slow and fast flow reservoirs is:

$$\frac{d(V_{s,pas}\delta_{s,pas})}{dt} = EGM_s \tag{11}$$

$$\frac{d(V_{f,pas}\delta_{f,pas})}{dt} = EGM_f \tag{12}$$

https://doi.org/10.5194/hess-2021-492
Preprint. Discussion started: 2 December 2021

Hydrology and Earth System Sciences
Open Access
Discussions

The above Eqs. (8) and (11) describe partial mixing between $V_s$ and $V_{s,pas}$ for the slow flow reservoir, and Eqs. (9) and (12) describe partial mixing between $V_f$ and $V_{f,pas}$ for the fast flow reservoir. Moreover, the partial mixing could be static or dynamic depending on whether the exchange coefficients between active and passive storages ($\varphi_s$ and $\varphi_f$) are constant or vary over time, respectively (Hrachowitz et al., 2013).

#### 3.1.3 Hillslope - depression connectivity and schematic model structures incorporating passive storage

The hillslope fast flow is assumed to fully connect with fast pathways in depression while the hillslope slow flow passes through the slow matrix in the depression. Therefore, $V_s$ and $V_f$ in the depression unit receive additional recharge from the hillslope slow flow ($\frac{A_h}{A_d}Q_s$) and fast flow ($\frac{A_h}{A_d}Q_f$), respectively, where $A_h$ and $A_d$ are hillslope and depression areas, respectively. Correspondingly, $V_s\delta_s$ and $V_f\delta_f$ in the depression are influenced by the isotope composition of inputs from the hillslope slow flow ($\frac{A_h}{A_d}Q_s\delta_s$) and fast flow ($\frac{A_h}{A_d}Q_f\delta_f$), respectively.

There is a dual drainage system comprising both a surface stream and underground channel in the depression. Here, we set a critical volume $V_m$ in the depression. The catchment flow drains from surface stream $Q_{sur}$ only when the depression groundwater storage meets: $V_{fd} > V_m$ (i.e., $Q_{sur} = \frac{(V_{fd} - V_m)A_d}{\Delta t}$). As a consequence, the total flow discharge at the catchment outlet $Q$ is composed of fast flow ($Q_f$) and slow flow ($Q_s$) in the subsurface, with additional contribution from the surface stream $Q_{sur}$.

https://doi.org/10.5194/hess-2021-492
Preprint. Discussion started: 2 December 2021




To assess the function of passive storage on simulating flow discharge and isotopic concentrations at the catchment outlet, we set fourteen schemes (scenarios) that incorporates 0~4 passive storages into different positions within the karst flow system, i.e., fast and/or slow flow reservoirs in combination with the hillslope and/or depression units (Table 3). The model parameters and their definitions are listed in Table 4.

**Table 3**. Different model structures that incorporate passive storages into fast flow and/or slow flow reservoirs at hillslope and/or depression units

| No. of Passive Storage | Model | Hillslope | | Depression | |
|---|---|---|---|---|---|
| | | Slow flow | Fast flow | Slow flow | Fast flow |
| 0 | *a* | - | - | - | - |
| 1 | *b* | √ | - | - | - |
| | *c* | - | √ | - | - |
| | *d* | - | - | √ | - |
| | *e* | - | - | - | √ |
| 2 | *f* | √ | √ | - | - |
| | *g* | - | - | √ | √ |
| | *h* | √ | - | √ | - |
| | *i* | - | √ | - | √ |
| 3 | *j* | √ | √ | √ | - |
| | *k* | √ | √ | - | √ |
| | *l* | - | √ | √ | √ |
| | *m* | √ | - | √ | √ |
| 4 | *n* | √ | √ | √ | √ |

Note： √ and - represent the fast/slow reservoir with and without an additional passive storage, respectively.

### 3.2 Model calibration and validation

In order to avoid over-parameterization, some insensitive parameters are fixed according to previous studies and field investigations. The ratio of matrix area to the area of hillslope or depression unit (α) is about 0.95 (Zhang et al., 2019; Zhang et al., 2020). *b* reflecting the degree of spatial heterogeneity of tension water storage

https://doi.org/10.5194/hess-2021-492
Preprint. Discussion started: 2 December 2021

Hydrology and Earth System Sciences Discussions

distribution is about 0.12 for small catchment (Xue et al., 2019). *wm* representing the holding capacity of moisture is 50 mm for thin soils over hillslope and 80 mm for thick soils over depression, respectively (Xue et al., 2019; Zhang et al., 2020). The volumes of passive storages ($W_{pas}$, $V_{s,pas}$ and $V_{f,pas}$) are generally one order of magnitude larger than those of active storage (Dunn et al., 2010, Soulsby et al., 2011, Ala-Aho et al, 2017). According to Eqs. (11) and (12), the passive storage volumes ($V_{s,pas}$ and $V_{f,pas}$) are dependent on the exchange coefficients between active and passive storages ($\varphi_s$ and $\varphi_f$). In this study, these passive storage volumes were set as as a constant (i.e., 300 mm) and the exchange coefficients are calibrated. Considering the rapid hydrological response of the fast flow system or hillslope unit to precipitation, the initial values of $V_{fh}$, $V_{fd}$ and $V_{sh}$ is set as 0 mm (Zhang et al., 2019), while the initial value of $V_{sd}$ is 20 mm (Xue et al., 2019). Meanwhile, the initial isotope rations are all initially set to the measurement at the catchment outlet (i.e., -61.3‰), this initialisation brings negligible errors since the isotope transport process is driven by rainfall inputs boundary condition. The undetermined model parameters (*kc*, *ks*, *Vm*, *ηs, ηf, ke* and *φ* in Table 4) are calibrated against observed discharge and isotope concentration.

The flow-isotope coupled models with different combinations of the active and passive storages (Table 3) were run on hourly time steps. The performance objective functions included the modified Kling-Gupta efficiency (KGE) and the absolute value of BIAS ($\text{Abias}_q$). KGE criterion comprehensively considers the linear correlation and

https://doi.org/10.5194/hess-2021-492
Preprint. Discussion started: 2 December 2021



standard deviation between the numerical and observed values (Kling et al., 2012) following:

$$KGE_i = 1 - \sqrt{(r-1)^2 + (std-1)^2 + (\sigma-1)^2} \tag{13}$$

where $r$ is the linear correlation coefficient between the simulated and observed values, $std$ is the ratio of the standard deviation of the numerical and observed values, and σ is the ratio of the average numerical value to the observed value, i = (q, c) representing the goodness of match for flow discharge or isotope concentration, respectively. The closer KGE is to 1, the better the overall performance of the coupled model.

The $\mathrm{Abias_q}$ is

$$\mathrm{Abias_q} = \left| \frac{\sum_{i=1}^{n}(S_i - O_i)}{O_i} \right| \tag{14}$$

where $S_i$ is the simulated discharge, and $O_i$ is the observed discharge. The closer $\mathrm{Abias_q}$ is to 0, the better performance of model in matching flow discharge at outlet.

In this study, the multi-objective optimization algorithm, i.e., non-dominated sorting genetic algorithm II (NSGA-II) proposed by Deb et al (2002), was applied for the model parameter calibration. The NSGA-II (Kollat and Reed, 2006) was based on NSGA algorithm representing the sets of pareto-optimal solutions. As pareto-optimal sets of solutions are not dominated by any one of factors as a result of trade-off effects, the "best" solution is achieved by satisfying the demands from all factors (e.g. $\mathrm{KGE_q}$, $\mathrm{KGE_c}$ and $\mathrm{Abias_q}$) (Fenicia et al., 2007). After a number of (e.g. 100 in this study) iterations of the NSGA-II algorithm, 30 final parameter sets were retained. The corresponding

https://doi.org/10.5194/hess-2021-492
Preprint. Discussion started: 2 December 2021



objective function values (average of the optimal solution sets) for both the calibration and validation periods were also extracted.

The observational data were used separately for the calibration and validation periods. That is, the model parameters were calibrated against the observed discharge and isotope concentration (δD) from October 8, 2016 to October 30, 2017. Note that since D and $^{18}O$ fluctuated with virtually the same dynamic over time, both driven by the same hydrological factors, therefore only D was used for calibration. Afterwards, the model was validated against observations from November 1, 2017 to June 14, 2018. The model parameter sets for the fourteen scenarios were obtained based on the 30 optimal solution sets for $KGE_q$, $KGE_c$ and $Abias_q$ in the calibration and validation periods (Fig. 5 and Table 5).

**Table 4.** The definitions of model parameters with their ranges and calibrated values

| Zone | Parameter and meaning | | Range | Calibrated |
|---|---|---|---|---|
| Area | $\alpha_h/\alpha_d$ | Ratio of matrix flow area | 0.95 | 0.95 |
| Unsaturated | $kc_h/ kc_d$ | Coefficient for evapotranspiration | 0.9~1.2 | 1.15/1.04 |
| | $ks_h/ ks_d$ | Ratio of water yield into slow flow reservoir | 0.1~0.5 | 0.24/0.31 |
| | $b_h/b_d$ | Exponential distribution of tension water capacity | 0.12 | 0.12 |
| | $wm_h/wm_d$ | Tension water storage capacity (mm) | 50/80 | 50/80 |
| | #Wpas | passive storage (mm) | 300 | 300 |
| Saturated | ~/ $Vm$ | Maximum storage of fast flow reservoir (mm) | 5~30 | 23 |
| | $\eta s_h/\eta s_d$ | Outflow coefficient of slow flow reservoir | 0.001~0.01 | 0.001/0.001 |
| | $\eta f_h/\eta f_d$ | Outflow coefficient of fast flow reservoir | 0.01~0.15 | 0.13/0.01 |
| | $ke_h/ ke_d$ | Exchange coefficient between slow and fast flow reservoirs ($10^{-4}$) | 0.1~1 | 0.3/0.7 |
| | #$\varphi_{sh}/\varphi_{sd}$ | Exchange coefficient between active and passive storages for slow flow | 0.1~0.5 | 0.26/NA |

https://doi.org/10.5194/hess-2021-492
Preprint. Discussion started: 2 December 2021



| | | | |
|---|---|---|---|
| # $\varphi_{fh}/\varphi_{fd}$ | Exchange coefficient between active and passive storages for fast flow | | 0.24/NA |
| # $V_{sh.pas}/V_{sd.pas}$ | Passive storage for slow flow (mm) | 300 | 300/300 |
| # $f_{fh.pas}/V_{fd.pas}$ | Passive storage for fast flow (mm) | | NA/NA |

Note: the upper and lower parameters and values in */* represent those in hillslope and depression, respectively; the parameters indicated by # refer to those used for isotope concentration simulation. NA represents not available.

## 4 Results and Discussion

### 4.1 Performance of models during calibration and validation periods

Our results (Table 5 and Fig. 5) show that most models obtain a higher $KGE_q$ but a lower $KGE_c$, though models *c*, *f*, *g* and *j* give both higher $KGE_q$ and $KGE_c$ (>0.5) in the calibration and validation periods. Particularly, the model *f* (adding two passive storages in the fast and slow flow reservoirs in the hillslope unit) performed the best in matching discharge and isotopic concentration. The average $KGE_q$ and $KGE_c$ from model *f* are higher than 0.6 in the calibration and validation periods and $Abias_q$ is relatively small (Table 5). Meanwhile, the model *f* gives a more constrained range of $KGE_q$, $KGE_c$ and $Abias_q$ from the 30 sets of optimal solutions (Fig. 5), further suggesting a lower uncertainty of the calibrated model parameters. The average isotope value of the outlet discharge simulated by model *f* is -61.5‰, with a range of -75.9~-36.3‰, which is close to the observed values (-61.3‰ for the average, and a range of -76.8~-45.5‰) in the calibration period. Moreover, model *f* can generally capture the flood peaks (Fig.6) and the isotope (δD) variations (Fig. 7).

The calibrated parameter values for the model *f* are listed in Table 4. These parameter values reasonably delineate the hydrological features of karst landforms. For example,

https://doi.org/10.5194/hess-2021-492
Preprint. Discussion started: 2 December 2021



the calibrated *ks* are 0.24 and 0.31 respectively for hillslope and depression units, suggesting about 80% of net precipitation recharging into fast flow reservoir through large fracture and sinkhole in terms of $I_f/R=(1-\alpha)P/R+(1-ks)\alpha$. The 80% of fast flow is consistent with the numerical results by Zhang et al (2011) independently derived using a distributed model that takes account of the role of sinkholes in facilitating fast flow recharge into the aquifer in the studied catchment. Worthington et al. (2000) also revealed that more than 90% of fast flow component in four typical karst aquifers in Kentucky, USA. The outflow coefficient of fast flow reservoir $\eta f$ (0.13/0.01 for the hillslope/depression in Table 4) is much greater than that of slow flow reservoir $\eta s$ (0.001/0.001), especially for the hillslope unit. This suggests that fast flow discharge is much more sensitive to active storage variability than slow flow discharge since $Q=\eta s \cdot V$. The large proportion of the fast flow component and significant variability in hillslope unit could result in pronounced mixing of isotope (D) signatures in various fractures and conduits due to dispersion and diffusion.

https://doi.org/10.5194/hess-2021-492
Preprint. Discussion started: 2 December 2021


Hydrology and Earth System Sciences
Open Access
Discussions

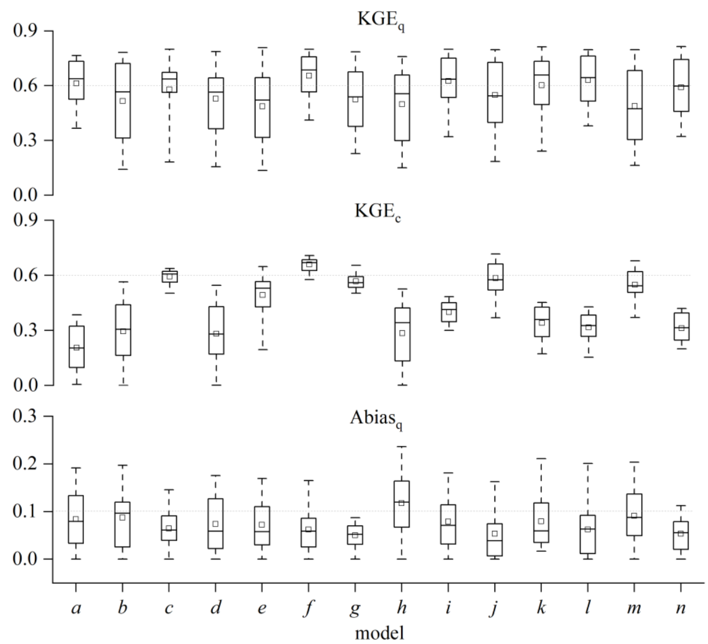


**Figure 5**. The box-plot of the 30 optimal solutions for the objective functions of $KGE_q$, $KGE_c$ and $Abias_q$ obtained from parameter calibration of 14 models

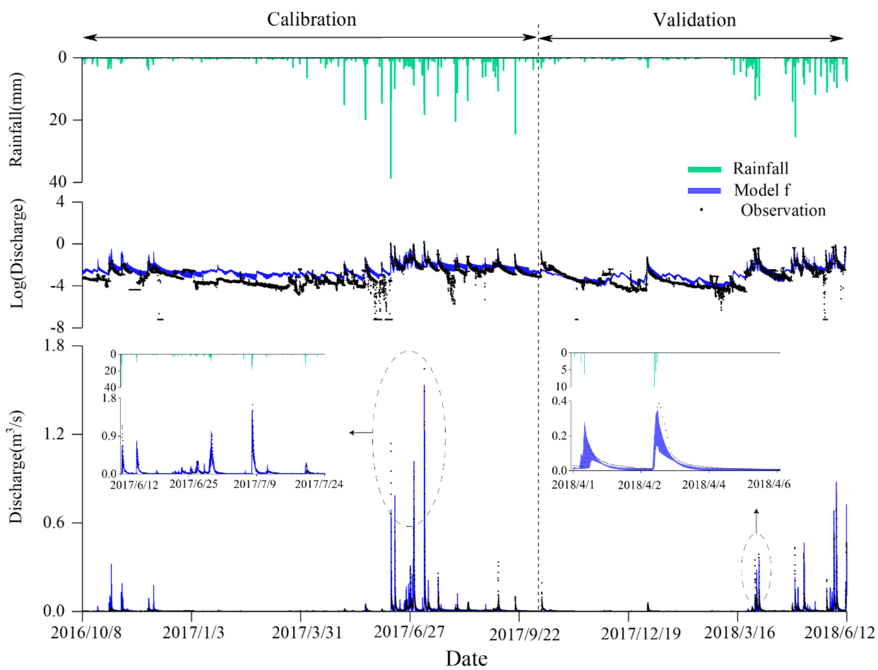

https://doi.org/10.5194/hess-2021-492
Preprint. Discussion started: 2 December 2021

Hydrology and Earth System Sciences
Discussions

**Figure 6**. Simulated discharge concentrations of the 30 sets of optimal solutions by model *f* in calibration and validation periods.

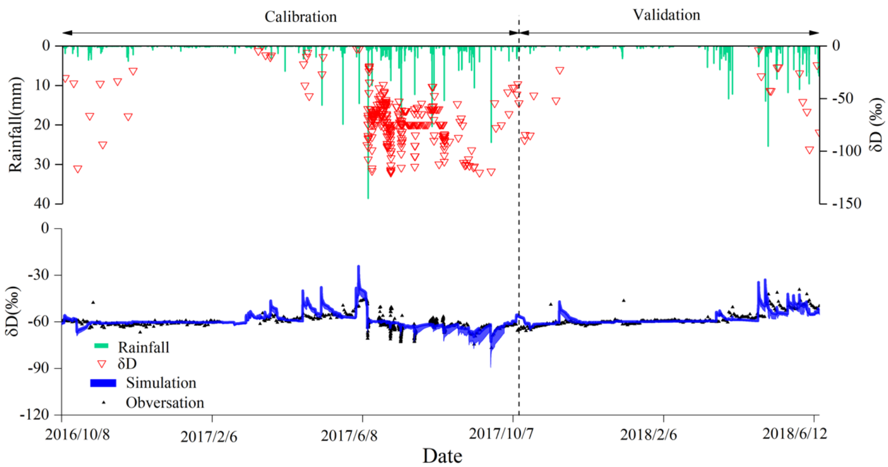


**Figure 7**. Simulated isotope concentrations of the 30 sets of optimal solutions by model *f* in calibration and validation periods.

**Table 5.** The model performance based on the average of 30 optimal solution sets for individual model structure

| No. of Passive Storage | Model | Calibration | | | Validation | | |
|---|---|---|---|---|---|---|---|
| | | $KGE_q$ | $KGE_c$ | $Abias_q$ | $KGE_q$ | $KGE_c$ | $Abias_q$ |
| 0 | ***a*** | **0.61** | **0.21** | **0.08** | **0.65** | **0.53** | **0.18** |
| 1 | *b* | 0.52 | 0.29 | 0.09 | 0.55 | 0.55 | 0.19 |
| | ***c*** | **0.58** | **0.59** | **0.06** | **0.61** | **0.64** | **0.18** |
| | *d* | 0.53 | 0.28 | 0.07 | 0.56 | 0.56 | 0.21 |
| | *e* | 0.52 | 0.49 | 0.07 | 0.50 | 0.69 | 0.20 |
| 2 | ***f*** | **0.65** | **0.66** | **0.04** | **0.68** | **0.63** | **0.18** |
| | *g* | 0.52 | 0.57 | 0.05 | 0.53 | 0.60 | 0.21 |
| | *h* | 0.50 | 0.28 | 0.12 | 0.55 | 0.55 | 0.19 |
| | *i* | 0.63 | 0.40 | 0.08 | 0.65 | 0.55 | 0.16 |
| 3 | ***j*** | **0.55** | **0.58** | **0.05** | **0.55** | **0.52** | **0.23** |
| | *k* | 0.60 | 0.34 | 0.08 | 0.64 | 0.43 | 0.15 |
| | *l* | 0.63 | 0.32 | 0.06 | 0.64 | 0.32 | 0.18 |
| | *m* | 0.49 | 0.55 | 0.09 | 0.53 | 0.57 | 0.17 |
| 4 | ***n*** | **0.59** | **0.31** | **0.05** | **0.60** | **0.31** | **0.20** |

https://doi.org/10.5194/hess-2021-492
Preprint. Discussion started: 2 December 2021

Hydrology and Earth System Sciences Discussions

**4.2 The effects of number of passive storages on flow and transport processes**

Functionally, the passive stores have negligible effects on water flow but mostly delay tracer transport through mixing. However, the models incorporating varying number of passive storages in different flow reservoirs and landscape units produced highly variable discharge simulations. This is demonstrated by the variations in $KGE_q$ (Table 5), i.e., $KGE_q$ values vary in the ranges of 0.49 to 0.65, and 0.50 to 0.68 in calibration and validation periods, respectively. The effect of different number of passive storages on discharge simulations can be attributed to the Pareto-optimal tradeoffs between the two objectives of $KGE_q$ and $KGE_c$ caused by the multi-objective calibration. For example, $KGE_q$ is negatively correlated with $KGE_c$ based on the 30 optimal solution sets by the NSGA-II algorithm (Fig. 8). Consequently, the multi-objective calibration gives a trade-off solution pair of 0.65 and 0.66 for $KGE_q$ and $KGE_c$, respectively, for the calibrated model *f*. As expect, the models with different number of passive storages affect extent of solute mixing and thus obtain different "best" simulated outlet isotope concentrations and the "highest" values of $KGE_c$ showed the tradeoffs between $KGE_c$ and $KGE_q$ through poorer stream flow simulations (Table 5).

On the other hand, increasing model parameterization through additional passive storage (e.g. the exchange coefficients of $\varphi_{sh}/\varphi_{sd}$ and $\varphi_{fh}/\varphi_{fd}$ in Table 4) alters the water flux exchange and isotope concentration allocations between slow flow and fast flow, which ultimately changes the relative contributions (proportion) of hydrological runoff components (i.e., slow flow, fast flow and surface flow) to the catchment outlet discharge. Here, in order to illustrate effects of the increasing model parameters on

https://doi.org/10.5194/hess-2021-492
Preprint. Discussion started: 2 December 2021



$KGE_c$ and $KGE_q$, we selected five representative models that incorporate 0~4 passive storages, respectively. Among these representative models (i.e., the most accurate model for a given number of passive storages), model *a* has no passive storage, and model *n* has 4 passive stores; the other three models, including model *c* (1 passive store ), *f* (2 passive store), and *j* (3 passive stores), give the highest $KGE_q$ and $KGE_c$ for each model group (Tables 3 and 5).

The partitioning of simulated outlet discharges by the five models are listed in Table 6. All models incorporating 0~4 passive storages have a high proportion of discharge from the fast flow system (i.e., fast flow discharge in hillslope, and the total of fast flow and surface flow discharges at catchment outlet in Table 6). In terms of the outlet flow discharge components, model *f* gives 52% of underground channel flow (the total amount of fast and slow flow) and 48% of surface stream flow, which are close to observed values at the underground channel (55%) and surface stream (45%), respectively. This is additional evidence that model *f* can faithfully capture observed flow discharge in the complex karst settings.

Effects of additional passive storages were also assessed by comparing contrasting pairs of numerical results with and without a passive storage in fast/slow flow reservoir. With an additional passive storage in fast flow reservoir, models (*c* and *n*) obtain a lower proportion of slow flow discharge and thus larger proportion of fast flow discharge. For example, model *c* obtains 20% and 18% of slow flow in the hillslope and depression units, respectively, less than the respective 26% and 23% of the benchmark model *a* (Table 6). Similarly, model *n* incorporates a passive storage in the fast flow reservoir for the depression unit. It gives 20% and 19% of the slow flow discharge in hillslope and depression units, respectively, less than 26% and 22% of the contrasting model *j*. The lower proportion of slow flow discharge and thus larger proportion of fast flow discharge given by model *c* and *n* result from the strengthened isotope mixing with an additional passive storage in fast flow reservoir that eventually leads to the enriched δD of fast flow and outlet discharge. This is supported by the fact that the δD of hillslope fast flow decreases from -61.6‰ for model *c* to -65.2‰ for model *a*, and δD of depression fast flow decreases from -61.5‰ for model *n* to -62.6‰ for model *j* (Table 7). Meanwhile, the δD of outlet discharge decreases correspondingly, while the means δD of slow flow in hillslope or depression unit from the contrasting models are nearly identical. Therefore, the enriched δD of outlet discharge due to the enrichment in fast flow suggests larger fast flow contributions and thus lower slow flow contributions.

In contrast, adding a passive storage in the slow flow reservoir gives a higher proportion of the slow flow discharge and lower fast flow contributions. This is supported by the numerical results for the contrasting pairs of models (e.g. model *j* vs. *f* in Table 6). That is, model *f* obtains 19% and 18% of the slow flow discharge in the hillslope and depression units, respectively, which are smaller than 26% and 22% of the slow flow discharge of model *j* with an additional passive storage in slow flow reservoir.

https://doi.org/10.5194/hess-2021-492
Preprint. Discussion started: 2 December 2021


Hydrology and Earth System Sciences
Discussions

The large variability of δD can be damped by incorporating passive storage in fast/slow flow reservoir, this is supported by the ranges of δD from the contrasting pairs of models. Adding more passive stores damps variability of δD and strengthens the enrichments of δD in almost all hydrological components. This is shown by the narrower ranges and less negative δD of the mean values at the outlet for models *c*, *f*, *j*, and *n* compared to the benchmark model *a* (Table 7). Consequently, the under-mixing with insufficient passive storage (e.g. models *a* and *c* in Table 7) cannot match the damped *δ*D values at the catchment outlet discharge. This is because: (a) the simulated δD variations by models *a* and *c* in Table 7 exceed the range of observed values (-76.8~-45.5‰), and (b) the simulated mean δD of flow discharge (-63.0 and -61.9‰ for models *a* and *c*, respectively, in Table 7) is more negative than the mean δD of observed values (-61.3‰).

On the other hand, over-mixing by adding more passive storages (e.g. models *j* and *n* in Table 7) leads to over-dampened δD values at the catchment outlet because the range of the simulated δD variability by models *j* and *n* are narrower than the range of observed values (Table 7). This further supports that model *f* with only two passive storages at hillslope might best capture the nature of the actual transport process in terms of the dispersion and mixing of the isotope inputs.

https://doi.org/10.5194/hess-2021-492
Preprint. Discussion started: 2 December 2021

Hydrology and Earth System Sciences
Discussions

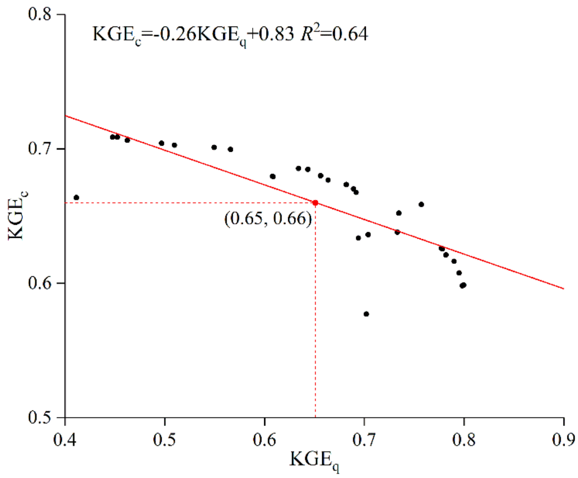


**Figure 8**. Relationship between $KGE_q$ and $KGE_c$ from the multi-objective calibration of model *f*.

**Table 6.** The proportions of flow components in the hillslope-depression-outlet continuum for the 30 optimal solution sets of the selected representative models during the calibration period (%)

| No. of Passive storage | Model | Hillslope | | | | Depression and catchment outlet | | | | | |
|---|---|---|---|---|---|---|---|---|---|---|---|
| | | Slow flow | | Fast flow | | Slow flow | | Fast flow | | Surface flow | |
| | | Range | Mean | Range | Mean | Range | Mean | Range | Mean | Range | Mean |
| 0 | *a* | 13~41 | 26 | 59~87 | 74 | 11~37 | 23 | 21~31 | 24 | 38~68 | 53 |
| 1 | *c* | 7~31 | 20 | 69~93 | 80 | 11~27 | 18 | 20~27 | 23 | 49~69 | 58 |
| 2 | *f* | 8~31 | 19 | 69~92 | 81 | 7~28 | 18 | 16~40 | 34 | 33~67 | 48 |
| 3 | *j* | 8~38 | 26 | 62~92 | 74 | 8~32 | 22 | 33~68 | 48 | 4~57 | 30 |
| 4 | *n* | 7~38 | 20 | 62~93 | 80 | 8~29 | 19 | 29~68 | 55 | 9~62 | 26 |

Note: the contrasting pairs of models (*c* vs. *a*, and *n* vs. *j*) reflect effect of fast flow reservoir with an additional passive storage on flow components; the contrasting pairs of models (*j* vs. *f*) reflect effects of slow flow reservoir with an additional passive storage on flow components.

https://doi.org/10.5194/hess-2021-492
Preprint. Discussion started: 2 December 2021

Hydrology and Earth System Sciences
Discussions

**Table 7.** The simulated isotope values (‰) of flow components in the hillslope-depression-outlet continuum for the 30 optimal solution sets from the selected representative models during the calibration period

| No. of Passive storage | Model | Hillslope | | | | Depression and catchment outlet | | | | | | | |
|---|---|---|---|---|---|---|---|---|---|---|---|---|---|
| | | Slow flow | | Fast flow | | Slow flow | | Fast flow/Surface flow | | Catchment outlet | | | |
| | | Range | Mean | Range | Mean | Range | Mean | Range | Mean | Range | Mean | Range (Observation) | Mean (Observation) |
| 0 | *a* | -67.7~-55.8 | -62 | -108.2~4.1 | -65.2 | -65.9~-58.6 | -61.5 | -104.2~-12.4 | -65.2 | -85.7~-22.0 | -63 | | |
| 1 | *c* | -67.3~-55.7 | -61.9 | -87.1~-6.8 | -61.6 | -66.5~-57.4 | -61.7 | -87.1~-34.5 | -62.4 | -78.4~-36.1 | -61.9 | | |
| 2 | *f* | -62.2~-57.2 | -59.9 | -87.3~-5.4 | -61.4 | -62.3~-58.4 | -60.6 | -85.3~-34.9 | -62.5 | -75.9~-36.3 | -61.5 | -76.8~-45.5 | -61.3 |
| 3 | *j* | -62.2~-57.3 | -60 | -87.4~-5.9 | -61.4 | -61.0~-59.2 | -60 | -90.2~-28.7 | -62.6 | -77.8~-33 | -61.6 | | |
| 4 | *n* | -62.8~-57 | -60 | -91.5~-1.5 | -61.7 | -61.4~-58.7 | -60 | -84~-27.9 | -61.5 | -77.2~-40 | -61.1 | | |

Note: the contrasting pairs of models (*c* vs. *a*, and *n* vs. *j*) reflect effects of fast flow reservoir with an additional passive storage on δD; the contrasting pairs of models (*j* vs. *f*) reflect effects of slow flow reservoir with an additional passive storage on δD.

https://doi.org/10.5194/hess-2021-492
Preprint. Discussion started: 2 December 2021



**4.3 The effects of position of passive storage on flow and transport processes**

The improved performance of simulations also strongly depends on the location of passive storages in the flow system. For example, the simulations of models *c* and *e* (with passive storage located in the hillslope/ depression fast flow reservoir) are better than those of model *b* and *d* (passive storage set in the hillslope/depression slow flow reservoir), and the simulations of model *f* (set passive storages in the slow and fast flow reservoirs of hillslope) are better than those of model *g* (with passive storages in the slow and fast flow reservoirs of depression). The importance of storage distribution has been reported in previous studies. Capell et al. (2012) initially used a tracer-aided model with four passive storages in upland and lowland units to simulate flows and tracer transport in the North Esk catchment in northeast Scotland. Their analysis identified only three passive storages were necessary, as the passive storage in shallow zone for the upland unit was negligible as sufficient damping was available in the dynamic (active) storage. Clearly, location of passive storage is an important component of model structure, while optimizing the number of storage balances minimizing model complexity and uncertainty, while still improving simulation performance of both flow and tracers.

Here, based on comparison of the 14 model performances, adding passive storage in the fast flow reservoir and the hillslope unit are more efficient for simulating flow and isotope dynamics. For instance, the models *c*, *f* and *j* with passive storage in the fast flow reservoir and/or hillslope unit obtains the highest simulation accuracy (the sum of $KGE_q$ and $KGE_c$ in Table 5) among the models incorporating 1~3 passive storages.

https://doi.org/10.5194/hess-2021-492
Preprint. Discussion started: 2 December 2021



Comparatively, model *f* incorporating passive storages into hillslope unit gives best overall simulations of outlet flow and isotopes.

**4.4 The dominant transport processes: advection, dispersion or molecular diffusion?**

Generally, the transport process is governed by advection with the tracer travelling with water, as well as molecular diffusion in a slow velocity (or immobile) zone, and by hydrodynamic dispersion in a fast velocity (or mobile) zone (Karadimitriou et al., 2016, Schumer et al., 2003, Wang et al., 2020). The dominance of such transport processes is often assessed by the Peclet number (*Pe*), a dimensionless metric defined as the ratio of advective flux to the dispersive/diffusive flux (Bear, 1972), which requires information about the dispersion coefficient. Zhao et al. (2019, 2021) used a transient storage model (TSM) to study the tailing of breakthrough curves (BTCs) of tracers in karst conduits, with experimental results suggesting that the dispersion coefficient was positively correlated not only with the flow velocity, but also with the number of storage zones. Fiori et al. (2008) also found that the dynamics of solutes in catchments are strongly influenced by the advective and dispersive processes. Indeed, the dominance of the hydrodynamic dispersion is widely found in the flow-conductive (preferential flow) zones (Roubinet et al., 2012).

Given the dominance of advection and dispersion over diffusion, the mass exchange flux (*EGM*) between active and passive storages should be dominated by the heterogeneity of the flow system. This is extreme in karst flow systems, where higher and lower flow velocity zones typically co-exist with strong heterogeneity between

https://doi.org/10.5194/hess-2021-492
Preprint. Discussion started: 2 December 2021



micropore, fracture and conduit media with permeability ranging across several orders of magnitude and the conductivity of the rock fractures decreasing with depth (Fig. 1d) (Zhang et al., 2011). In these circumstances, the spatial variations in advection speed are a major mechanism underlying macro-dispersion at catchment scale (Kirchner et al., 2001).

Both the hillslope and depression units represent large-scale heterogeneities in subsurface conductivity, but the depression unit has a higher flow velocity and the longer flow paths to the outlet. Tracers landing farther from the stream at the hillslope unit will undergo more dispersion (Kirchner et al., 2001). In terms of the Peclet number $Pe = vL/2D$ ($L$ is the hillslope/depression length, $v$ is the advective velocity, and $D$ is the diffusion constant), $Pe$ for the hillslope flow could be much larger than that for the depression flow. Therefore, the macro-dispersion at the hillslope unit could dominate subsurface transport. The effect of the dominated dispersion on solute mixing at the hillslope unit is supported by large *EGM* in Table 8. Adding passive storages in the hillslope unit with mechanical mixing has a major effect on isotope transport, which significantly improves model performance.

**Table 8.** The simulated $|EGM|$ ($m^3$ ‰) of flow components in the hillslope-depression-outlet continuum for the 30 optimal solution sets from the selected representative models during the calibration period

| No. of Passive storage | Model | Hillslope | | | | Depression and catchment outlet | | | |
|---|---|---|---|---|---|---|---|---|---|
| | | Slow flow | | Fast flow | | Slow flow | | Fast flow | |
| | | Range | Mean | Range | Mean | Range | Mean | Range | Mean |
| 1 | *c* | NA | NA | 0~72460 | 101 | NA | NA | NA | NA |
| 2 | *f* | 0~19463 | 25 | 0~60737 | 99 | NA | NA | NA | NA |

https://doi.org/10.5194/hess-2021-492
Preprint. Discussion started: 2 December 2021



| | | | | | | | | | |
|---|---|---|---|---|---|---|---|---|---|
| 3 | *j* | 0~38362 | 35 | 0~61267 | 98 | 0~4799 | 7 | NA | NA |
| 4 | *n* | 0~31391 | 26 | 0~43947 | 89 | 0~6324 | 7 | 0~8985 | 46 |

Note: NA represents not available.

## 5 Conclusions

In this study, we developed and tested a coupled flow-tracer model for simulating discharge and isotope signatures for the cockpit karst landscapes represented as a “hillslope-depression-outlet” continuum. We tested 14 simulation cases with alternative model structures by varying the number and locations of passive storage in the fast/slow flow reservoirs of hillslope/depression units. The model structures and parameters were optimized by using a multi-objective optimization algorithm to match the observed discharge and isotope dynamics in the Chenqi catchment of southwest China.

We found that models with additional passive storages can improve performance in matching isotope dynamics to some extent. In the study catchment, an optimal model structure was found incorporate only two passive storages in both the fast and slow flow reservoirs in the hillslope unit. Adding only one or more than two passive storages achieves suboptimal results that is supported by the values of $KGE_q$, $KGE_c$ and $Abias_q$.

The optimal model structure reflects that the outlet discharge and tracer dynamics are mostly controlled by flow and transport processes in the hillslope. Moreover, since the hillslope fast flow system contributes about 82% of the outlet discharge, and the mean δD (-61.5‰) and variation of the catchment outlet discharge is close to that of hillslope fast flow (-61.4‰). Consequently, we propose that transport process in the

https://doi.org/10.5194/hess-2021-492
Preprint. Discussion started: 2 December 2021


Hydrology and Earth System Sciences
Open Access
Discussions

Chenqi catchment are dominated by advection and dispersion processes mediated by the heterogeneity of flow systems.

Characterizing the dynamics of flow paths in complex geological settings, and considering active and passive zones the hillslopes and depressions of karst landscapes, is central for better understanding fluid flow and solute transport processes. This study provided evidence that the protection of hillslope environments is significant for the prevention of disasters, such as droughts, floods and contamination in karst landscapes.

**Acknowledgment:** This research was supported by the National Natural Science Foundation of China (42030506).

**Data availability:** The discharge and isotope data that support the findings of this study can be shared after the ending of our project according to the project executive policy. Anyone who would like to use the data can contact the corresponding author.

**Code availability:** The code that support the findings of this study is available from the corresponding author upon reasonable request.

**Declaration of Competing Interest:** I declare that neither I nor my co-authors have any competing interest.

**References:**

Ala-Aho, P., Tetzlaff, D., Mcnamara, J.P., Laudon, H., Soulsby, C.: Using isotopes to constrain water flux and age estimates in snow-influenced catchments using the

https://doi.org/10.5194/hess-2021-492
Preprint. Discussion started: 2 December 2021

Hydrology and Earth System Sciences
Open Access
Discussions

STARR (Spatially distributed Tracer-Aided Rainfall-Runoff) model, Hydrol. Earth Syst. Sci., 21, 5089-5110, https://doi.org/10.5194/hess-21-5089-2017, 2017.

Aquilina, L., Ladouche, B., Dörfliger, N.: Water storage and transfer in the epikarst of karstic systems during high flow periods, J. Hydrol., 327, 472-485, https://doi.org/10.1016/j.jhydrol.2005.11.054, 2006.

Batiot, C., Emblanch, C., Blavoux, B.: Total Organic Carbon (TOC) and magnesium ($Mg^{2+}$): two complementary tracers of residence time in karstic systems, C. R. Geosci., 335, 205-214, https://doi.org/10.1016/S1631-0713(03)00027-0, 2003.

Bear, J.: Dynamics of Fluids in Porous Media, Dover Publications, Mineola, New York, 1972.

Beven, K.: A manifesto for the equifinality thesis, J. Hydrol., 320, 18-36, https://doi.org/10.1016/j.jhydrol.2005.07.007, 2006.

Birkel, C., Soulsby, C., Tetzlaff, D.: Modelling catchment-scale water storage dynamics: reconciling dynamic storage with tracer-inferred passive storage, Hydrol. Process., 25(25), 3924-3936, https://doi.org/10.1002/hyp.8201, 2011.

Birkel, C., Soulsby, C.: Advancing tracer-aided rainfall-runoff modelling: A review of progress, problems and unrealised potential, Hydrol. Process., 29, 5227-5240, https://doi.org/10.1002/hyp.10594, 2015.

Capell, R., Tetzlaff, D., Soulsby, C.: Can time domain and source area tracers reduce uncertainty in rainfall-runoff models in larger heterogeneous catchments? Water Resour. Res., 48, W09544, https://doi.org/10.1029/2011wr011543, 2012.

https://doi.org/10.5194/hess-2021-492
Preprint. Discussion started: 2 December 2021


Carey, S., Quinton, W.: Evaluating snowmelt runoff generation in a discontinuous permafrost catchment using stable isotope, hydrochemical and hydrometric data, Hydrol. Res., 35, 309-324, https://doi.org/10.2166/nh.2004.0023, 2004.

Chacha, N., Njau, K.N., Lugomela, G.V., Muzuka, A.N.N.: Groundwater age dating and recharge mechanism of Arusha aquifer, northern Tanzania: application of radioisotope and stable isotope techniques, Hydrogeol. J., 26, 2693-2706, https://doi.org/10.1007/s10040-018-1832-0, 2018.

Chang, Y., Hartmann, A., Liu, L., Jiang, G., Wu, J.: Identifying more realistic model structures by electrical conductivity observations of the karst spring, Water Resour. Res., 57, e2020WR028587. https://doi.org/10.1029/2020WR028587, 2020.

Chen, X., Zhang, Z., Soulsby, C., Cheng, Q., Binley, A., Jiang, R., Tao, M.: Characterizing the heterogeneity of karst critical zone and its hydrological function: an integrated approach, Hydrol. Process., 2018, 32, 2932-2946, https://doi.org/10.1002/hyp.13232, 2018.

Deb, K., Pratap, A., Agarwal, S., Meyarivan, T.: A fast and elitist multi-objective genetic algorithm: NSGA-II. IEEE Trans. Evol. Comput., 6, 182-197, https://doi.org/10.1109/4235.996017, 2002.

Dunn S.M., Birkel, C., Soulsby, C., Tetzlaff, D.: Transit time distributions of a conceptual model: their characteristics and sensitivities, Hydrol. Process., 24, 1719-1729, https://doi.org/10.1002/hyp.7560, 2010.

https://doi.org/10.5194/hess-2021-492
Preprint. Discussion started: 2 December 2021




Elghawi, R., Pekhazis, K., Doummar, J.: Multi-regression analysis between stable isotope composition and hydrochemical parameters in karst springs to provide insights into groundwater origin and subsurface processes: regional application to Lebanon, Environ. Earth Sci., 80, 1-21, https://doi.org/10.1007/s12665-021-09519-4, 2021.

Fenicia, F., Savenije, Hubert.H.G., Matgen, P., Pfister, L.: A comparison of alternative multiobjective calibration strategies for hydrological modeling, Water Resour. Res., 43, W03434, https://doi.org/10.1029/2006wr005098, 2007.

Fenicia, F., Wrede, S., Kavetski, D., Pfister, L., Hoffmann, L., Savenije, H.H.G., McDonnell, J.J.: Assessing the impact of mixing assumptions on the estimation of streamwater mean residence time, Hydrol. Process., 24, 1730-1741, https://doi.org/10.1002/hyp.7595, 2010.

Fiori, A., Russo, D.: Travel time distribution in a hillslope: Insight from numerical simulations, Water Resour. Res., 44, W12426, http://doi.org/10.1029/2008WR007135, 2008.

Hrachowitz, M.; Savenije, H.; Bogaard, T. A.; Tetzlaff, D.; Soulsby, C.: What can flux tracking teach us about water age distribution patterns and their temporal dynamics?, Hydrol. Earth Syst. Sci., 17, 533-564, https://doi.org/10.5194/hess-17-533-2013, 2013.

Hartmann, A., Barberá, J.A., Lange, J., Andreo, B., Weiler, M.: Progress in the hydrologic simulation of time variant recharge areas of karst systems-Exemplified at a karst spring in Southern Spain, Adv. Water Resour., 54, 149-160, https://doi.org/10.1016/j.advwatres.2013.01.010, 2013.

He, Z., Unger-Shayesteh, K., Vorogushyn, S., Weise, S.M., Kalashnikova, O., Gafurov, A., Duethmann, D., Barandun, M., Merz, B.: Constraining hydrological model parameters using water isotopic compositions in a glacierized basin, central Asia, J. Hydrol., 571, 332-348, https://doi.org/10.1016/j.jhydrol.2019.01.048, 2019.

Kirchner, J.W., Feng, X., Neal, C.: Catchment-scale advection and dispersion as a mechanism for fractal scaling in stream tracer concentrations, J. Hydrol., 254, 82-101, https://doi.org/10.1016/s0022-1694(01)00487-5, 2001.

Kling, H., Fuchs, M., Paulin, M.: Runoff conditions in the upper Danube basin under an ensemble of climate change scenarios, J. Hydrol., 424, 264-277, https://doi.org/10.1016/j.jhydrol.2012.01.011, 2012.

Kollat, J.B., Reed, P.M.: Comparing state-of-the-art evolutionary multi-objective algorithms for long-term groundwater monitoring design, Adv. Water Resour., 29, 792-807, https://doi.org/10.1016/j.advwatres.2005.07.010, 2006.

Karadimitriou, N.K., Joekar-Niasar, V., Babaei, M., Shore, C.A.: Critical Role of the Immobile Zone in Non-Fickian Two-Phase Transport: A New Paradigm. Environ. Sci. Technol., 50, 4384-4392, https://doi.org/10.1021/acs.est.5b05947, 2016.

Long, A.J., Putnam, L.D.: Linear model describing three components of flow in karst aquifers using $^{18}$O data, J. Hydrol., 296, 254-270, https://doi.org/10.1016/j.jhydrol.2004.03.023, 2004.

https://doi.org/10.5194/hess-2021-492
Preprint. Discussion started: 2 December 2021



Mart ńez‑Santos, P., Andreu, J.M.: Lumped and distributed approaches to model natural recharge in semiarid karst aquifers, J. Hydrol., 388, 389-398, https://doi.org/10.1016/j.jhydrol.2010.05.018, 2010.

Min, Z., Y, Hu., Cheng, Z., Liu, Z., Yang, R., Chen, B.: Effects of land cover on variations in stable hydrogen and oxygen isotopes in karst groundwater: A comparative study of three karst catchments in Guizhou Province, Southwest China, J. Hydrol., 565, 374-385, https://doi.org/10.1016/j.jhydrol.2018.08.037, 2018.

Nan, Y., Tian, L., He, Z., Tian, F., Shao, L.: The value of water isotope data on improving process understanding in a glacierized catchment on the Tibetan Plateau. Hydrol. Earth Syst. Sci., https://doi.org/10.5194/hess-2021-134, 2021.

Page, T., Beven, K. J., Freer, J., Neal, C.: Modelling the chloride signal at Plynlimon, Wales, using a modified dynamic TOPMODEL incorporating conservative chemical mixing (with uncertainty), Hydrol. Process., 21, 292-307, https://doi.org/10.1002/hyp.6186, 2007.

Perrin, C., Michel, C., AndreÂassian, V.: Does a large number of parameters enhance model performance? Comparative assessment of common catchment model structures on 429 catchments, J. Hydrol., 242, 275-301. https://doi.org/10.1016/S0022-1694(00)00393-0, 2001.

Plummer, L.N., Busenberg, E., McConnell, J.B., Drenkard, S., Schlosser, P., Michel, R.L.: Flow of river water into a Karstic limestone aquifer. 1. Tracing the young fraction in groundwater mixtures in the Upper Floridan Aquifer near Valdosta,

https://doi.org/10.5194/hess-2021-492
Preprint. Discussion started: 2 December 2021

Hydrology and Earth System Sciences
Discussions

Georgia, Appl. Geochem., 13, 995-1015, https://doi.org/10.1016/S0883-2927(98)00031-6, 1998.

Qin, D., Zhao, Z., Guo, Y., Liu, W., Haji., Wang, X., Xin, B., L, Y., Yang, Y.: Using hydrochemical, stable isotope, and river water recharge data to identify groundwater flow paths in a deeply buried karst system, Hydrol. Process., 31, 4297-4314, https://doi.org/10.1002/hyp.11356, 2017.

Roubinet, D., Dreuzy, J., Tartakovsky, D.M.: Semi-analytical solutions for solute transport and exchange in fractured porous media, Water Resour. Res., 48, 273-279, https://doi.org/10.1029/2011WR011168, 2012.

Soulsby, C., Piegat, K., Seibert, J., Tetzlaff, D.: Catchment scale estimates of flow path partitioning and water storage based on transit time and runoff modelling, Hydrol. Process., 25, 3960-3976, https://doi.org/10.1002/hyp.8324, 2011.

Sprenger, M., Tetzlaff, D., Soulsby, C.: Soil water stable isotopes reveal evaporation dynamics at the soil-plant-atmosphere interface of the critical zone, Hydrol. Earth Syst. Sci., 21, 3839-3858, https://doi.org/10.5194/hess-21-3839-2017, 2017.

Sprenger, M., D. Tetzlaff, J. Buttle, H. Laudon, H. Leistert, C.P.J. Mitchell, J. Snelgrove, M. Weiler, and C. Soulsby.: Measuring and modeling stable isotopes of mobile and bulk soil water, Vadose Zone J., 17, 170149, https://doi.org/10.2136/vzj2017.08.0149, 2018.

Stadnyk, T.A., Delavau, C., Kouwen, N., Edwards, T.W.D.: Towards hydrological model calibration and validation: simulation of stable water isotopes using the

https://doi.org/10.5194/hess-2021-492
Preprint. Discussion started: 2 December 2021

Hydrology and Earth System Sciences
Discussions
Open Access

isoWATFLOOD model, Hydrol. Process., 27, 3791-3810, https://doi.org/10.1002/hyp.9695, 2013.

Streltsova, T.D.: Hydrodynamics of groundwater flow in a fractured formation, Water Resour. Res., 12, 405-414, https://doi.org/10.1029/WR012i003p00405, 1976.

Schumer, R., Benson, D.A., Meerschaert, M.M., Baeumer, B.: Fractal mobile/immobile solute transport, Water Resour. Res., 39(10), 1296, https://doi.org/10.1029/2003WR002141, 2003.

Wang, L., Cardenas, M. B., Zhou, J.Q., Ketcham, R. A.: The complexity of nonlinear flow and non-Fickian transport in fractures driven by three-dimensional recirculation zones, J. Geophys. Res.-Solid Earth., 125, e2020JB020028, https://doi.org/10.1029/2020JB020028, 2020.

White, W.B.: A brief history of karst hydrogeology: contributions of the NSS, J. Cave Karst Stud., 69, 13-26, 2007.

Worthington, S.R.H., Davies, G.J., Ford, D.C., Sasowsky I.D.(eds), Wicks C.M.(des): Matrix, fracture and channel components of storage and flow in a Paleozoic limestone aquifer. Groundwater flow and contaminant transport in carbonate aquifers. Balkema Publications, Rotterdam, The Netherlands, 2000.

Worthington S.R.H.: Diagnostic hydrogeologic characteristics of a karst aquifer (Kentucky, USA), Hydrogeol. J., 17, 1665-1678, https://doi.org/10.1007/s10040-009-0489-0, 2009.

https://doi.org/10.5194/hess-2021-492
Preprint. Discussion started: 2 December 2021


Hydrology and Earth System Sciences Discussions
Open Access

Xue, B., Chen, X., Zhang, Z., Cheng, Q.: A Semi-distributed Karst Hydrological Model Considering the Hydraulic Connection Between Hillslope and Depression: a case Study in Chenqi Catchment. China Rural Water And Hydropower, 437, 1-5, 2019. (In Chinese)

Zhang, Z., Chen, X., Ghadouani, A., Peng, S.: Modelling hydrological processes influenced by soil, rock and vegetation in a small karst basin of southwest China, Hydrol. Process., 25, 2456-2470, https://doi.org/10.1002/hyp.8022, 2011.

Zhang, Z., Chen, X., Chen, X., Shi, P.: Quantifying time lag of epikarst-spring hydrograph response to rainfall using correlation and spectral analyses. Hydrogeol. J., 21, 1619-1631, https://doi.org/10.1007/s10040-013-1041-9, 2013.

Zhang, R., Chen, X., Zhang, Z., Soulsby, C.: Using hysteretic behavior and hydrograph classification to identify hydrological function across the "hillslope-depression-stream" continuum in a karst catchment. Hydrol. Process., 34, 3464-3480, https://doi.org/10.1002/hyp.13793, 2020.

Zhang, Z., Chen, X., Cheng, Q., Soulsby, C.: Storage dynamics, hydrological connectivity and flux ages in a karst catchment: conceptual modelling using stable isotopes, Hydrol. Earth Syst. Sci., 23, 51-71, https://doi.org/10.5194/hess-23-51-2019, 2019.

Zhao, R.J.: The xinanjiang model applied in china. J. Hydrol., 135, 371-381, https://doi.org/10.1016/0022-1694(92)90096-E, 1992.

Zhao, X., Chang, Y., Wu, J., Xue, X.: Effects of flow rate variation on solute transport in a karst conduit with a pool. Environ. Earth Sci., 78, 237, https://doi.org/10.1007/s12665-019-8243-y, 2019.

Zhao, X., Chang, Y., Wu, J., Li, Q., Cao, Z.: Investigating the relationships between parameters in the transient storage model and the pool volume in karst conduits through tracer experiments, J. Hydrol., 593, 125825, https://doi.org/10.1016/j.jhydrol.2020.125825, 2021.